Hindawi
Journal of Electrical and Computer Engineering
Volume 2020, Article ID 7516578, 13 pages
https://doi.org/10.1155/2020/7516578

Research Article

Multi-Time Scale Optimal Dispatch for AC/DC Distribution Networks Based on a Markov Chain Dynamic Scenario Method and MPC

Jie Liu[1], **Xingquan Ji**[1], **Kejun Li**[2] **and Kaiyuan Zhang**[1]

[1]*College of Electrical Engineering and Automation, Shandong University of Science and Technology, Qingdao 266590, China*
[2]*Institute of Renewable Energy and Smart Grid, Shandong University, Jinan 250061, China*

Correspondence should be addressed to Xingquan Ji; xqji@sdust.edu.cn

Received 20 July 2019; Revised 12 September 2019; Accepted 31 January 2020; Published 20 February 2020

Academic Editor: Yagang Zhang

A multi-time scale optimal dispatch model based on the scenario method and model predictive control (MPC) in the AC/DC distribution network is established due to the uncertainty of wind and load. A Markov chain dynamic scenario method is proposed, which generates scenarios by characterizing the forecast error via empirical distribution. Considering the time correlation of the forecast error, Markov chain is adopted in the Markov chain dynamic method to simulate the uncertainty and variability in wind and load with time. A multi-time scale optimal dispatch strategy based on MPC is proposed. The operation scheduling of operation units is solved in day-ahead and intraday optimal dispatch by minimizing the expected value of total cost in each scenario. In the real-time optimal dispatch, the stability and robustness of system operation are considered. MPC is adopted in the real-time optimal dispatch, taking the intraday scheduling as reference and using the roll optimization method to compute real-time optimal dispatch scheduling to smooth the output power. The simulation results in a 50-node system with uncontrollable distributed energy demonstrate that the proposed model and strategy can effectively eliminate fluctuations in wind and load in AC/DC distribution networks.

1. Introduction

1.1. Motivation. An active distribution network (ADN) has advantages in actively adjusting power flow, managing variable distributed energy, and improving the efficiency of distributed energy [1–4]. As an important part of the ADN, the AC/DC distribution network is a significant development trend of future distribution networks and has better efficiency in supplying the DC load [5–8]. The DC network has better energy quality and longer transmission distance than the AC network. The energy storage system (ESS) and some distributed generation (DG) must be connected to the AC distribution network by a voltage source converter (VSC); if the dc distribution network is used for power supply, a large number of converters will be saved and energy loss will be reduced [9–11].

Distributed energy is a significant component of the AC/DC distribution network. The output power of some types, such as wind and solar, fluctuates and is uncontrollable, and the forecast accuracy decreases sharply with increasing time scale. It is important to reasonably schedule the output power of controllable distributed energy to account for uncontrollable energy. Methods based on stochastic programming have been widely adopted to address the uncertainty of uncontrollable energy output, and scenario-based programming is the most commonly used stochastic programming method [12]. The main idea is to generate scenarios according to the character of the fluctuations of uncertain factors, making the decision variable meet the requirements in all scenarios. In [13], a scenario method and chance-constrained programming were proposed to establish a multi-time rolling dispatch model to optimize the configuration of variable resources. In [14], a two-stage reactive power optimization of the distribution network based on extreme scenario was applied using extreme scenario constraints to deal with unknown variables. In [15], a

dynamic scenario method was proposed to generate a dynamic scenario with correlation according to the analysis of historical data.

In [16], a multi-time scale optimal dispatch method was applied since the accuracy of wind turbine and load prediction gradually increased with time scale subdivision, and this method effectively increased the proportion of wind turbine consumption. In [17], a multi-time active power coordination scheduling method was proposed based on the idea of level by level subdivision and mutual coordination to correct the error between the forecast value and the actual value in the next layer. Unlike the traditional time scale subdivision, model predictive control (MPC) adopts the roll optimization method to subdivide the time scale and considers the feedback correction of the control process, which can address the fluctuation of controllable distributed energy well. The traditional multi-time scale optimal methods have slow response speed which may lead to a large forecast error. In [18], MPC was used for handling plug-and-play charging requests of flexible loads in a distribution system. In [19], MPC was applied to control voltage in the ADN according to roll optimization of unknown variables. In [20], a method based on D-MPC was proposed to control the voltage of wind farms, which aimed to coordinate the wind turbine and the static reactive power generator and optimize the process of reactive power adjustment to smooth the future voltage curve. In [21], a multi-time scale optimal dispatch method based on MPC was applied which using roll optimization strategy to replace the time scale subdivision optimal dispatch method.

1.2. Contribution. In order to better deal with the uncertainty of wind power and improve the prediction precision, a multi-time scale optimal dispatch model based on Markov chain dynamic scenario method and MPC for the AC/DC distribution network is proposed in this paper, and the main contributions are as follows:

(1) The distribution of the forecast error is generally assumed as normal distribution and beta distribution, which is a relatively simple way to simulate the uncertainty of wind power without using historical error data. However, it is concluded that normal distribution and beta distribution cannot be used to model the measured power for its given data sets because the great variety of the forecast methods and applied locations would lead to different approximate theoretical distributions or even no theoretical distribution [22]. In order to better describe the uncertainty of wind power, the Markov chains dynamic scenario method is adopted to generate scenarios, which estimate the covariance matrix of the multivariate normal distribution to fit the distribution of historical wind power fluctuations and adopt an inverse transform sampling method from a multivariate normal distribution to generate scenarios. Additionally, considering the time correlation of the forecast error, a Markov chain model is formulated to simulate the change process of the forecast error probability distribution with time, which can effectively ensure the reliability of generated scenarios when the prediction time scale is long.

(2) Traditional multi-time scale optimization methods mainly focus on cost optimization without further consideration of system stability. In order to better ensure the stability of system, an MPC-based multi-time scale optimal dispatch strategy is proposed. In the day-ahead and intraday dispatch, the scenario-based method is adopted to deal with the uncertainty of wind power. The on-off state of device, the grid purchase decision, the output power of regular device, and the expected power of the fast response device are solved in day-ahead and intraday optimal dispatch by minimizing the expected value of total cost in each scenario. The system stability is mainly considered in real-time optimal dispatch since most of the costs have been optimized. The expected power of the fast response device solved in the day-ahead and intraday dispatch is taken as the reference to minimize the difference between the solved control variables and the expected value by roll optimization and feedback correction. Therefore, in real-time optimal dispatch, it is only necessary to adjust the output power of fast response device appropriately based on the expected value according to the measured wind power, which can not only meet the load power of system but also solve the problem of volatility of DG power, thus improving the stability of system.

2. Markov Chain Dynamic Scenario Method

Markov chain dynamic scenario method characterizes forecast error via empirical distributions of a set of forecast bins, using Markov chain to simulate the change process of forecast error distribution, and the inverse transform is adopted to generate scenario according to the historical forecast error distribution, which ensure the reliability of generated scenarios, and the main steps are as follows:

(1) Processing historical data: collecting historical data of wind and load to obtain the data pairs (measured, forecast) and transform the value of the data to per-unit values.

(2) Generating the forecast bins: choose 50 bins with 0.02 pu bin widths in this case, and every forecast has a corresponding measurement, which is assigned to the same bin as the forecast. Then, sorting the data pairs (measured, forecast) by the forecast values and assigned to the matching forecast power bins to obtain the forecast error distribution of each random variable in each forecast bin.

(3) Discretizing the forecast error distribution of each random variable into seven intervals centered on the zero mean, with a width equal to the standard deviation δ. The state of the corresponding interval i is

denoted as $x_i\,(i = 1, 2, \ldots, 7)$, and the occurrence probability of this state interval is S_i. All the probability $S_{i.k.t}\,(i = 1, 2, \ldots, 7)$ of the k-th forecast bin at moment t constitutes the error state vector $\mathbf{P}_{k.t}$ at the current time. The expressions are as follows:

$$\mathbf{P}_{k.t} = [S_{1.k.t}, S_{2.k.t}, \ldots, S_{7.k.t}], \tag{1}$$

$$\sum_{i=1}^{7} S_{i.k.t} = 1. \tag{2}$$

(4) Generating the probability density function $\mathrm{F}_{k.t}(X)$ in each forecast bin according to the error state vector in the forecast bins. The expression is as follows:

$$F_{k.t}\left(x_j\right) = \sum_{i=1}^{j} S_{i.k.t}, \quad j = 1, 2, \ldots, 7. \tag{3}$$

(5) Generating random vectors [15]: generate Z random vectors $\mathbf{Y} = \{Y_1, Y_2, \ldots, Y_l\}$ with zero mean and standard deviation, which follows a multivariate normal distribution. The structure of $\boldsymbol{\Sigma}$ is as follows:

$$\boldsymbol{\Sigma} = \begin{bmatrix} \sigma_{1.1} & \sigma_{1.1} & \cdots & \sigma_{1.l} \\ \sigma_{2.1} & \sigma_{2.1} & \cdots & \sigma_{2.l} \\ \vdots & \vdots & \ddots & \vdots \\ \sigma_{l.1} & \sigma_{l.2} & \cdots & \sigma_{l.l} \end{bmatrix}, \tag{4}$$

where l is the length of the generated scenario sequence and $\sigma_{m.n}$ is the covariance of Y_m and Y_n, which can be expressed as

$$\sigma_{m.n} = \mathrm{cov}\left(Y_m, Y_n\right) = e^{-((|m-n|)/\varepsilon)}, \quad 0 \le n, m \le \Delta t, \tag{5}$$

where ε is the range parameter controlling the strength of the correlation of the random variable sequence.

(6) Generating error scenarios [15]: the inverse transform shown in (6) is used to transform a random vector following a multivariate normal distribution into an error vector with correlation to generate an error scenario within the forecast time:

$$\Delta\omega_t = F_{i.k}^{-1}\left(\Phi\left(Y_t\right)\right), \tag{6}$$

where $\Delta\omega_t$ is the generated forecast error at moment t and $\Phi(Y_t)$ is the cumulative density function following a normal distribution, which is

$$\Phi\left(Y_t\right) = \int_{-\infty}^{Y_t} \frac{\exp\left(-x^2/2\right)}{\sqrt{2\pi}} \mathrm{d}x. \tag{7}$$

Following these steps above, the multivariate normal random variable is converted into scenarios following both the marginal distribution of wind power forecast error among the forecast horizon. But the prediction precision will decrease with the growth in prediction time scale when the forecast horizon is long. Wind and load power within a day need to be predicated in the day-ahead dispatch, so the time correlation of forecast error should be considered. For the good performance of the Markov chain shown in the simulation of wind and load output sequences [23, 24], the Markov chain is incorporated into the traditional dynamic scenario method. The change process of the forecast error probability distribution with time is regarded as a Markov chain, which is a stochastic process of transition from one state to another. In this paper, the state transition matrix is generated according to the historical forecast error data. The state transition is utilized to update the forecast error probability distribution in each forecast bin at set intervals when the prediction time scale is long, which can effectively ensure the reliability of generated scenarios. The main steps are as follows.

(7) Forming the state transition matrix: the state transition matrix is the most important part in the whole Markov chain process, and the expression is as follows:

$$\mathbf{E}_{k.t} = \begin{bmatrix} E_{11} & E_{1.1} & \cdots & E_{1.n} \\ E_{2.1} & E_{2.1} & \cdots & E_{2.n} \\ \vdots & \vdots & \ddots & \vdots \\ E_{n.1} & E_{n.2} & \cdots & E_{n.n} \end{bmatrix}_{n \times n}, \tag{8}$$

where $\mathbf{E}_{k.t}$ is the state transition matrix of the k-th forecast bin at moment t and E_{mn} is the state transition probability from the state x_m in the last moment to the state x_n in the next moment, which is

$$E_{mn} = \frac{N_{mn}}{\sum_{j=1}^{n} N_{mj}}, \tag{9}$$

where N_{mn} is the number at which the state x_m in the last moment transits to the state x_n in the next moment through the statistics of historical data of unknown variables.

(8) Generating the error state of all forecast cases: after obtaining the state transition matrix, the state transition matrix is used to generate the error state of all the forecast cases in the next period and then return to Step (4) to continue scenario generation. The expression is as follows:

$$\mathbf{P}_{k.t+1} = \mathbf{P}_{k.t}\mathbf{E}_{k.t}. \tag{10}$$

3. Multi-Time Scale Optimal Strategy

The uncertainty of wind turbines brought new challenges for multi-time scale optimal dispatch in the AC/DC distribution network. Considering that the prediction precision will increase with a shortened time scale, a multi-time scale optimal coordinate dispatch strategy is adopted, as shown in

Figure 1, in which the dispatching process is divided into three stages: day-ahead, intraday, and real time [25]. Microturbines are classified into regulation microturbines (RMTs) and quick-adjustment microturbines (QAMTs) according to the response speed:

(1) Day-ahead scheduling: the scheduling cycle is 24 hours, and the time interval is 1 hour. The Markov chain dynamic scenario method is adopted to generate the scenario, and the time interval of the Markov chain process is 4 hours. The on-off state of RMT and QAMT is solved in day-ahead optimal dispatch by minimizing the expected value of total cost in each scenario.

(2) Intraday scheduling: the scheduling cycle is 1 hour, and the time interval is set to 15 minutes. The dynamic scenario method is adopted to generate the forecast scenario since the intraday time scale is not long, and the time correlation of forecast error can be ignored. The RMT output power and the grid purchase decision are solved in intraday optimal dispatch by minimizing the expected value of total cost in each scenario.

(3) Real-time scheduling: the scheduling cycle is 15 minutes, and the time interval is 5 minutes. Considering the stability of system, MPC is adopted to compute output power of QAMT and ESS by taking the intraday scheduling as reference and using roll optimization method and feedback correction.

4. Multi-Time Scale-Coordinated Optimization Model

4.1. Day-Ahead Optimization Model

4.1.1. Objective Function. The objective function of day-ahead optimal dispatch is to minimize the expected value of total cost in each scenario, which is

$$\min\left(\begin{array}{l}\sum_{t=1}^{N_t} c_{\text{grid}.t}\sum_{s=1}^{N_s}\pi_s P_{\text{grid}.s.t}+\sum_{t=1}^{N_t}\sum_{i=1}^{N_{DG.F}}\left(\sum_{s=1}^{N_s}\pi_s C^F_{DG.i.s.t}+U^F_{DG.i.t}+D^F_{DG.i.t}\right)+\\ \quad\sum_{t=1}^{N_t}\sum_{i=1}^{N_{DG.R}}\sum_{s=1}^{N_s}\left(\pi_s C^R_{DG.i.s.t}+U^R_{DG.i.t}+D^R_{DG.i.t}\right)+\\ \quad\sum_{t=1}^{N_t}\sum_{i=1}^{N_{\text{ESS}}}\sum_{s=1}^{N_s}\left(\pi_s C_{\text{ESS}.i.s.t}\right)+\sum_{t=1}^{N_t}\sum_{i=1}^{N_{\text{wt}}}\sum_{s=1}^{N_s}\left(\pi_s\lambda^{\text{curt}}_{i.s.t}W^{\text{curt}}_{i.s.t}\right)\end{array}\right)\Delta t, \tag{11}$$

where N_t is the dispatching cycle; $N_{DG.F}$ is the number of QAMT; $N_{DG.R}$ is the number of RMT; N_s is the number of the scenarios; N_{ESS} is the number of ESSs; N_{wt} is the number of wind turbines; $c_{\text{grid}.t}$ is the electricity price at moment t; $P_{\text{grid}.s.t}$ is the exchange power between ADN and the upper grid at moment t in scenario s; $C^F_{DG.i.s.t}$ is the power cost of QAMT i at moment t in scenario s; $U^F_{DG.i.t}$ and $D^F_{DG.i.t}$ are the cost of starting and stopping, respectively, QAMT i at moment t; $C^R_{DG.i.s.t}$ is the power cost of RMT i at moment t in scenario s; $U^R_{DG.i.t}$ and $D^R_{DG.i.t}$ are the starting and stopping costs, respectively, of RMT i at moment t; $C_{\text{ESS}.i.s.t}$ is the power cost of ESS i at moment t in scenario s; $W^{\text{curt}}_{i.s.t}$ is the cutting wind quantity of wind turbine i at moment t in scenario s; $\lambda^{\text{curt}}_{i.s.t}$ is the cutting wind cost of wind turbine i at moment t in the scenario s; π_s is the probability of the scenario s; and Δt is the time interval.

4.1.2. Main Constraints

(1) Power balance constraints:

$$\sum_{i=1}^{N_{DG.F}} P^F_{DG.i.s.t}+\sum_{i=1}^{N_{DG.R}} P^R_{DG.i.s.t}+\sum_{i=1}^{N_{\text{wt}}}\left(P_{wt.i.s.t}-W^{\text{curt}}_{i.s.t}\right)+\sum_{i=1}^{N_{\text{ESS}}} P_{\text{ESS}.i.s.t}+P_{\text{grid}.s.t}-P_{\text{loss}.s.t}-R_{s.t}=P_{\text{load}.s.t}, \tag{12}$$

where $P^F_{DG.i.s.t}$ is the power of QAMT i at moment t in scenario s, $P^R_{DG.i.s.t}$ is the power of RMT i at moment t in scenario s, $P_{\text{wt}.i.s.t}$ is the power of wind turbine i at moment t in scenario s, $P_{\text{ESS}.i.t}$ is the power of ESS i at moment t in scenario s, $P_{\text{load}.s.t}$ is the load power at moment t in scenario s, $P_{\text{loss}.s.t}$ is the power loss in the AC/DC distribution network at moment t in scenario s, and $R_{s.t}$ is the spinning reserve in the scenario s at moment t [14].

(2) Power limit constraints:

$$u^F_{i.s.t}P^F_{DG.i.\min}\le P^F_{DG.i.s.t}\le u^F_{i.s.t}P^F_{DG.i.\max}, \tag{13}$$

$$u^R_{i.s.t}P^R_{DG.i.\min}\le P^R_{DG.i.s.t}\le u^R_{i.s.t}P^R_{DG.i.\max}, \tag{14}$$

where $P^F_{DG.i.\max}$ and $P^F_{DG.i.\min}$ are the upper limit and lower limit of the power of QAMT i, respectively; $u^F_{i.t}$ is the on-off state of QAMT i at moment t; $P^R_{DG.i.\max}$ and $P^R_{DG.i.\min}$ are the upper limit and lower limit of the power of RMT i, respectively; and $u^R_{i.t}$ is the on-off state of RMT i at moment t.

(3) On-off state constraints:

$$x^F_{i.t}+y^F_{i.t}\le 1, \tag{15}$$

$$x^F_{i.t}-y^F_{i.t}=u^F_{i.t}-u^F_{i.t-1}, \tag{16}$$

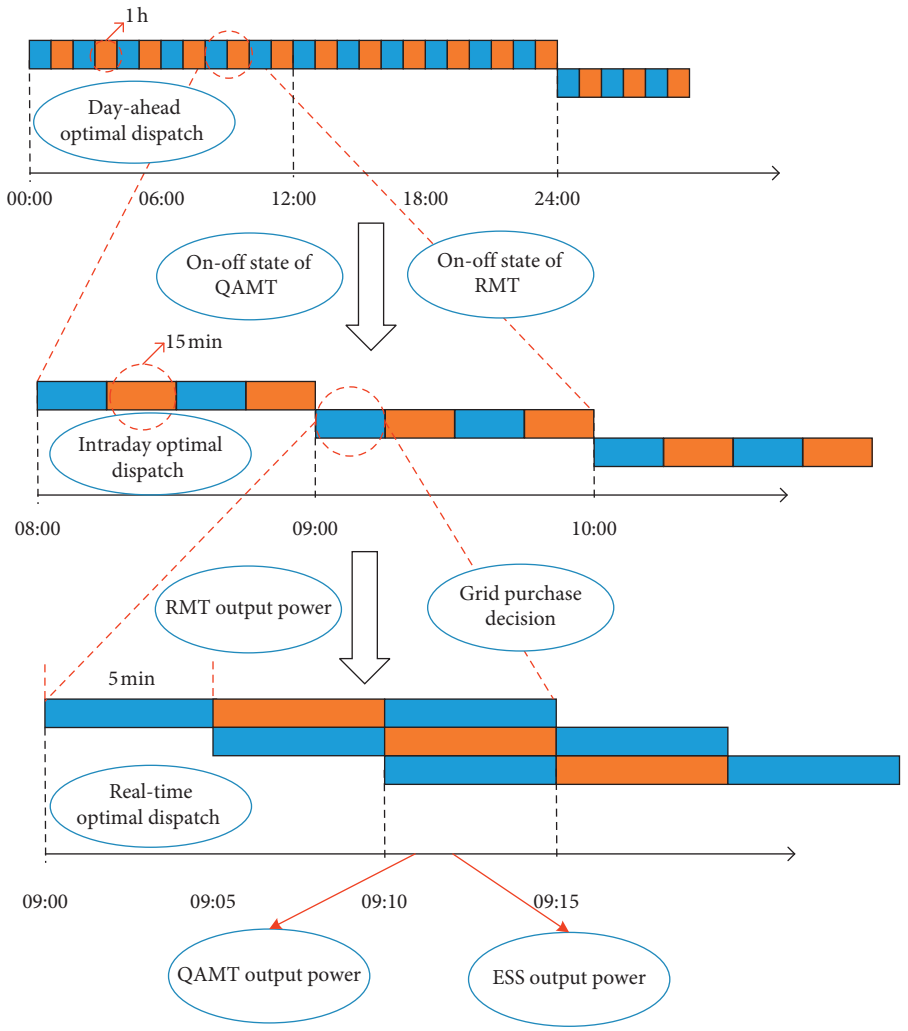

Figure 1: Multi-time scale optimization process.

$$x_{i.t}^{R} + y_{i.t}^{R} \le 1, \tag{17}$$

$$x_{i.t}^{R} - y_{i.t}^{R} = u_{i.t}^{R} - u_{i.t-1}^{R}, \tag{18}$$

where $x_{i.t}^{F}$ and $y_{i.t}^{F}$ are the starting and stopping action, respectively, of QAMT i and $x_{i.t}^{R}$ and $y_{i.t}^{R}$ are the starting and stopping action, respectively, of RMT i.

(4) Climbing constraints:

$$\begin{cases} \left|P_{DG.i.s.t}^{R} - P_{DG.i.s.t-1}^{R}\right| \le \left|u_{i.t}^{R} - u_{i.t-1}^{R}\right| P_{DG.i.\min}^{R} + \Delta_{i}^{R}, \\ \left|P_{DG.i.s.t}^{F} - P_{DG.i.s.t-1}^{F}\right| \le \left|u_{i.t}^{F} - u_{i.t-1}^{F}\right| P_{DG.i.\min}^{F} + \Delta_{i}^{F}, \end{cases} \tag{19}$$

where Δ_{i}^{R} and Δ_{i}^{F} are the climbing rate of RMT and QAMT, respectively.

(5) VSC converter station constraints:

The AC part and the DC part are connected through the VSC, and the connecting point can be assumed as a virtual node [26], as shown in Figure 2. In Figure 2, $P_{ac.ij.s.t}$, $Q_{ac.ij.s.t}$, and $P_{dc.jk.s.t}$ are the active power in the AC part, reactive power in the AC part, and active power in the DC part in scenario s at moment t, respectively; $Q_{vsc.j.s.t}$ is the reactive power of VSC in scenario s at moment t; $R_{vsc.ij}$ is the equivalent resistance of the loss in the converter station; $X_{vsc.ij}$ is the equivalent reactance of the filter in the converter station; $U_{ac.i.s.t}$ is the voltage at the AC side in scenario s at moment t; $U_{dc.k.s.t}$ is the voltage at the DC side in scenario s at moment t; and $U_{vsc.j.s.t}$ is the voltage of the VSC virtual node in scenario s at moment t.

According to the equivalent circuit in Figure 2, we obtain

$$P_{ac.ij.s.t} - \frac{\left(\left(P_{ac.ij.s.t}\right)^{2} + \left(Q_{ac.ij.s.t}\right)^{2}\right)}{\left(U_{ac.s.i}\right)^{2}} R_{vsc.ij} = P_{dc.jk.s.t}, \tag{20}$$

$$Q_{ac.ij.s.t} - \frac{\left(\left(P_{ac.ij.s.t}\right)^2 + \left(Q_{ac.ij.s.t}\right)^2\right)}{\left(U_{ac.s.i}\right)^2} X_{vsc.ij} = -Q_{vsc.j.s.t}, \tag{21}$$

$$-Q_{vsc.j.\max} \le Q_{vsc.j.s.t} \le Q_{vsc.j.\max}, \tag{22}$$

$$U_{vsc.s.j} = U_{ac.s.i} - 2\left(P_{ac.ij.s.t}R_{vsc.ij} + Q_{ac.ij.s.t}X_{vsc.ij}\right) + \frac{\left(\left(P_{ac.ij.s.t}\right)^2 + \left(Q_{ac.ij.s.t}\right)^2\right)\left(\left(R_{vsc.ij}\right)^2 + \left(X_{vsc.ij}\right)^2\right)}{\left(U_{ac.s.i}\right)^2}, \tag{23}$$

$$U_{vsc.s.j} = \frac{\sqrt{3}}{3}\mu M_i U_{dc.s.k}, \tag{24}$$

where $Q_{vsc.j.\max}$ and $-Q_{vsc.j.\max}$ are the upper limit and lower limits, respectively, of the power of VSC j; μ is the efficiency of dc voltage ($0 \le \mu \le 1$, μ is set to 0.866 when the modulation mode is SPWM); and M_i is the modulation of VSC i ($0 \le M_i \le 1$).

(6) ESS operation constraints:

$$\begin{cases} S_{\text{ESS}.i.s.t} = S_{\text{ESS}.i.s.t-1}\left(1 - \varepsilon_{\text{ESS}}\right) - \dfrac{P_{\text{ESS}.i.s.t}\Delta t}{E_{s.i}\eta_d}, \\ \qquad\qquad P_{\text{ESS}.i.s.t} > 0, \\ S_{\text{ESS}.i.s.t} = S_{\text{ESS}.i.s.t-1}\left(1 - \varepsilon_{\text{ESS}}\right) - \dfrac{\eta_c P_{\text{ESS}.i.s.t}\Delta t}{E_{s.i}}, \\ \qquad\qquad P_{\text{ESS}.i.s.t} < 0, \end{cases} \tag{25}$$

$$S_{\text{ESS}.i.\min} \le S_{\text{ESS}.i.s.t} \le S_{\text{ESS}.i.\max}, \tag{26}$$

$$-P_{\text{ESS}.i.\max} \le P_{\text{ESS}.i.s.t} \le P_{\text{ESS}.i.\max}, \tag{27}$$

$$S_{\text{ESS}.i.s.T} = S_{\text{ESS}.i.s.1}, \tag{28}$$

where $S_{\text{ESS}.i.s.t}$ is the energy of ESS i at moment t in scenario s; $P_{\text{ESS}.i.s.t}$ is the power of ESS i at moment t in scenario s; η_d and η_c are the efficiency of discharge and charge, respectively; $E_{s.i}$ is the capacity of ESS i in scenario s; $S_{\text{ESS}.i.\max}$ and $S_{\text{ESS}.i.\min}$ are the upper limit and lower limits, respectively, of the capacity of ESS i; ε_{ESS} is the ESS self-discharge; and $P_{\text{ESS}.i.\max}$ is the upper limit of the power of ESS i.

4.1.3. Day-Ahead Optimal Dispatch Result. The starting and stopping plan of QAMT $u^R_{i.s.t}$ and the starting and stopping plans of RMT $u^F_{i.s.t}$ in the next day are determined through day-ahead optimal dispatch, which are taken as input data in the intraday optimal dispatch model to compute other unknown variables in the intraday optimal dispatch model.

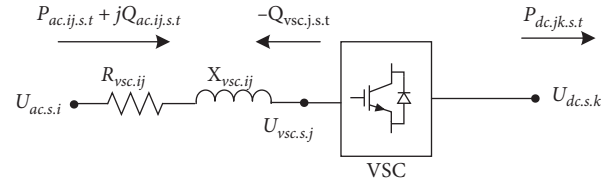

Figure 2: VSC converter station model.

4.2. Intraday Optimal Model

4.2.1. Objective Function. The objective function of intraday optimal dispatch is to minimize the expected value of total cost in each scenario, which is

$$\min \sum_{t=1}^{N_t}\sum_{i=1}^{N_{DG.F}} C^F_{DG.i.t} + \sum_{t=1}^{N_t}\sum_{i=1}^{N_{DG.R}}\sum_{s=1}^{N_s}\left(\pi_s C^R_{DG.i.s.t}\right) + \sum_{t=1}^{N_t}\sum_{i=1}^{N_{\text{ESS}}}\sum_{s=1}^{N_s}\left(\pi_s C_{\text{ESS.i.s.t}}\right) + \sum_{t=1}^{N_t}\sum_{i=1}^{N_{\text{wt}}}\sum_{s=1}^{N_s}\left(\pi_s \lambda^{\text{curt}}_{i.s.t} W^{\text{curt}}_{i.s.t}\right). \tag{29}$$

4.2.2. Main Constraints

(1) Power balance constraints:

$$\sum_{i=1}^{N_{DG.F}} P^F_{DG.i.s.t} + \sum_{i=1}^{N_{DG.R}} P^R_{DG.i.t} + \sum_{i=1}^{N_{\text{wt}}}\left(P_{\text{wt}.i.s.t} - W^{\text{curt}}_{i.s.t}\right) + \sum_{i=1}^{N_{\text{ESS}}} P_{\text{ESS}.i.s.t} + P_{\text{grid}.t} - P_{\text{loss}.s.t} - R_{s.t} = P_{\text{load}.s.t}, \tag{30}$$

where $P^R_{DG.i.t}$ is the power of RMT i at moment t and $P_{\text{grid}.t}$ is the exchange power between ADN and the upper grid at moment t.

The remaining constraints of the intraday optimization model are the same as the constraints of the day-ahead optimal dispatch, and the operation states of QAMT and RMT are obtained by the day-ahead optimal dispatch.

4.2.3. Intraday Optimal Dispatch Result. The power scheduling of RMT and the grid purchase decision, the expected value of QAMT, and ESS are determined through intraday optimal dispatch; these values are taken as inputs in the real-time optimal dispatch model to compute other unknown variables.

4.3. Real-Time Optimal Dispatch Model

4.3.1. MPC. Model predictive control is a finite domain closed-loop optimal control algorithm based on the prediction model. The main idea is as follows: in each sample moment, the prediction model is established to compute optimal control variable according to objective function and constraints, and the control variable at the current moment is issued. Then, the feedback correction is adopted for the issued control variable to modify the control variable [27].

The MPC-based optimal dispatch method is utilized to minimize the difference between the solved control variables in the future and the expected value of the control variables solved in the day-ahead optimal dispatch considering the network constraints by using roll optimization and feedback correction, which samples every 5 minutes, and the process is shown in Figure 3. The actual values of QAMT and ESS at the current sampling time are taken as the original state to compute the control command sequence in the next 15 minutes and issue the control instructions in the first 5 minutes, and the process is repeated at the next sampling time, which can not only meet the load demand of the system but also keep the issued adjustment value from getting too high. Additionally, the closed-loop control is formed due to the feedback correction part, which can further increase the prediction precision to ensure the stability of system.

4.3.2. Establishing Prediction Model. The prediction model is adopted to predict output power of QAMT, ESS, and the grid in the next period to compute the control variable, which are as follows [19]:

$$\begin{cases} \mathbf{P}_{\mathrm{DG}}(k+i\,|\,k) = \mathbf{P}_{\mathrm{DG0}}(k) + \sum_{t=1}^{i} \Delta\mathbf{u}_{\mathrm{DG}}(k+t\,|\,k), \quad i = 1, 2, \ldots, N, \\ \mathbf{P}_{\mathrm{ESS}}(k+i\,|\,k) = \mathbf{P}_{\mathrm{ESS0}}(k) + \sum_{t=1}^{i} \Delta\mathbf{u}_{\mathrm{ESS}}(k+t\,|\,k), \quad i = 1, 2, \ldots, N, \end{cases} \tag{31}$$

where N is the prediction step and $\mathbf{P}_{\mathrm{DG0}}(k)$ and $\mathbf{P}_{\mathrm{ESS0}}(k)$ are the original value of QAMT and ESS measured in the sampling time, respectively. $\Delta\mathbf{u}_{\mathrm{DG}}(k+t\,|\,k)$ and $\Delta\mathbf{u}_{\mathrm{ESS}}(k+t\,|\,k)$ are the power increments of QAMT and ESS in the next period predicted at moment k, respectively; $\mathbf{P}_{\mathrm{DG}}(k+i\,|\,k)$ and $\mathbf{P}_{\mathrm{ESS}}(k+i\,|\,k)$ are the power of QAMT and ESS in the next period predicted at moment k, respectively.

4.3.3. Objective Function. The objective is to minimize the deviation between the issued control command sequence and the expected value of intraday optimal dispatch, which is

$$\begin{aligned} &\min\left(\mathbf{P}_{\mathrm{DG.pre}} - \mathbf{P}_{\mathrm{DG.ref}}\right)^{T} \mathbf{W} \left(\mathbf{P}_{\mathrm{DG.pre}} - \mathbf{P}_{\mathrm{DG.ref}}\right) \\ &\quad + \left(\mathbf{P}_{\mathrm{ESS.pre}} - \mathbf{P}_{\mathrm{ESS.ref}}\right)^{T} \mathbf{Q} \left(\mathbf{P}_{\mathrm{ESS.pre}} - \mathbf{P}_{\mathrm{ESS.ref}}\right), \end{aligned} \tag{32}$$

where $\mathbf{W}$ is the weight coefficient matrix of QAMT, $\mathbf{Q}$ is the weight matrix of ESS, $\mathbf{P}_{\mathrm{DG.pre}}$ is the power of QAMT in the future $k+i$ times predicted in the sampling time, and $\mathbf{P}_{\mathrm{ESS.pre}}$ is the power of ESS in the future $k+i$ times predicted in the sampling time, which is

$$\begin{cases} \mathbf{P}_{\mathrm{DG.pre}} = \left[\mathbf{P}_{\mathrm{DG}}(k+1\,|\,k), \mathbf{P}_{\mathrm{DG}}(k+2\,|\,k), \ldots, \mathbf{P}_{\mathrm{DG}}(k+N\,|\,k)\right]^{T}, \\ \mathbf{P}_{\mathrm{ESS.pre}} = \left[\mathbf{P}_{\mathrm{ESS}}(k+1\,|\,k), \mathbf{P}_{\mathrm{ESS}}(k+2\,|\,k), \ldots, \mathbf{P}_{\mathrm{ESS}}(k+N\,|\,k)\right]^{T}, \end{cases} \tag{33}$$

$$\begin{aligned} \mathbf{P}_{\mathrm{DG}}(k+i\,|\,k) = \big[&P_{\mathrm{DG.1}}(k+i\,|\,k), P_{\mathrm{DG.2}}(k+i\,|\,k), \ldots, \\ &\cdot P_{\mathrm{DG.N_{DG}}}(k+i\,|\,k)\big], \end{aligned} \tag{34}$$

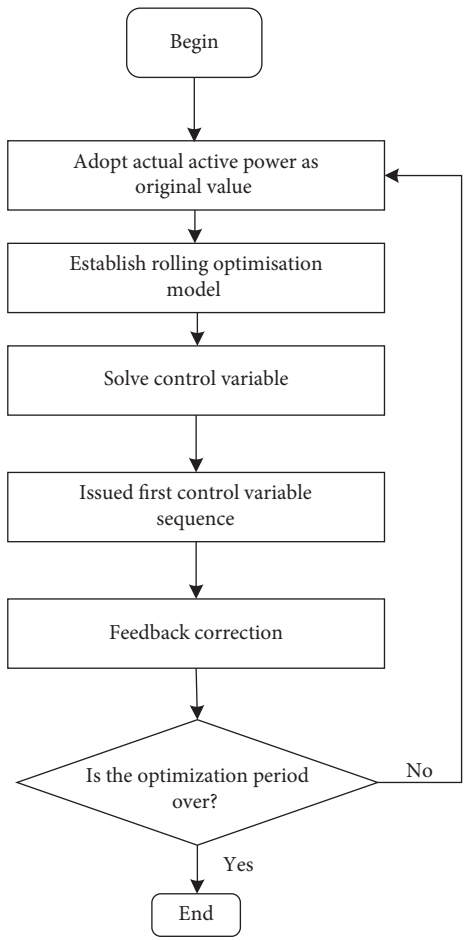

Figure 3: Real-time optimal dispatch process.

$$\begin{aligned} \mathbf{P}_{\mathrm{ESS}}(k+i\,|\,k) = \big[&P_{\mathrm{ESS.1}}(k+i\,|\,k), P_{\mathrm{ESS.2}}(k+i\,|\,k), \ldots, \\ &\cdot P_{\mathrm{ESS.N_{ESS}}}(k+i\,|\,k)\big], \end{aligned} \tag{35}$$

where $\mathbf{P}_{\mathrm{DG.ref}}$ is the expected value of QAMT in intraday optimal dispatch from sampling time to time $k+N$ and $\mathbf{P}_{\mathrm{grid.ref}}$ is the expected value of ESS in intraday optimal dispatch from sampling time to time $k+N$, which is

$$\begin{cases} \mathbf{P}_{\mathrm{DG.ref}} = \left[\mathbf{P}_{\mathrm{DG.ref}}^{T}(k+1\,|\,k), \mathbf{P}_{\mathrm{DG.ref}}^{T}(k+2\,|\,k), \ldots, \right. \\ \qquad\qquad \left. \mathbf{P}_{\mathrm{DG.ref}}^{T}(k+N\,|\,k)\right]^{T}, \\ \mathbf{P}_{\mathrm{ESS.ref}} = \left[\mathbf{P}_{\mathrm{ESS.ref}}^{T}(k+1\,|\,k), \mathbf{P}_{\mathrm{ESS.ref}}^{T}(k+2\,|\,k), \ldots, \right. \\ \qquad\qquad \left. \mathbf{P}_{\mathrm{ESS.ref}}^{T}(k+N\,|\,k)\right]^{T}. \end{cases} \tag{36}$$

4.3.4. Issuing Instruction. The control command sequence of QAMT and ESS in the future N moment is solved by the real-time optimization model:

$$\left\{\Delta\mathbf{u}^{T}(k+1\,|\,k), \Delta\mathbf{u}^{T}(k+2\,|\,k), \ldots, \Delta\mathbf{u}^{T}(k+N\,|\,k)\right\}. \tag{37}$$

The first command is issued in the control increment sequence to compute the power of QAMT and ESS in the AC/DC distribution network in the next period:

$$\mathbf{P}(k+1\mid k) = \mathbf{P}_0(k) + \Delta\mathbf{u}^T(k+1\mid k). \tag{38}$$

4.3.5. Feedback Correction. The measured value at current sampling time is taken as the original value of the new roll optimization before the next roll optimization to avoid the interference caused by the uncertainty of the wind turbine. The feedback formula is as follows [19]:

$$\mathbf{P}_0(k+1) = \mathbf{P}_{\text{real}}(k+1) + \delta, \tag{39}$$

where $\mathbf{P}_0(k+1)$ is the original power in the time $k+i$, $\mathbf{P}_{\text{real}}(k+1)$ is the actual measured power in the time $k+i$, and δ is the measured error.

The remaining constraints of the real-time optimization model are the same as those of the day-ahead optimal dispatch, and the expected value of QAMT and ESS, the RMT power, and the grid purchase decision is obtained by intraday optimal dispatch.

4.3.6. Real-Time Optimal Dispatch Result. The control command sequence of QAMT and ESS, the output power of QAMT and ESS, and the storage state of ESS are determined through real-time optimal dispatch.

5. Case Study

The Yalmip and Cplex solvers are used for modeling and solving the optimal dispatch model. The test is performed on a PC with an Intel Core (TM) i5-3340s CPU@2.8 GHz processor and 8 GB of memory.

The simulation is conducted on a 50-node AC/DC distribution network, as shown in Figure 4 [28]. WT is the wind turbine unit, DG_F is the QAMT, DG_R is the RMT, and ESS is the energy storage system. The RMT with an upper limit of power of 300 kW is connected to nodes 10 and 37, and the QAMT with an upper limit of power of 300 kW is connected to nodes 18 and 46, with a power factor of 0.9. ESS with an upper limit of power of 300 kW and energy storage of 1800 kWh is connected to nodes 36 and 49, and ESS with an upper limit of power of 240 kW and energy storage of 1400 kWh is connected to nodes 41 and 45. The time-of-use electricity price is adopted, which is shown in Figure 5.

One thousand scenarios for wind and load are generated in intraday dispatch and day-ahead dispatch, respectively, and then these original scenarios are reduced to 5 scenarios for wind and load by the K-means clustering method [29], so the number of total scenarios is 25. The generated scenario is applied to the wind and load data of EirGrid in 2017 and 2018. Figures 6 and 7 are the reduced wind scenario and the reduced load scenario, respectively, generated in the day-ahead dispatch. The wind and load scenarios are generated by the forecast value and forecast error sampled from the empirical cumulative distribution function using the transformation in (6). It is observed that the load scenarios have lower volatility than the wind scenarios, and this is because the forecast error of load is much smaller than that of wind power in the historical data. Additionally, it is shown that the wind output power is low from 2:00 to 6:00, so the demand of microturbine output power and exchange power is high. From 7:00 to 12:00, with the sharp increase in wind output power and the growth of load power is relatively low, the demand of microturbine output power and exchange power begins to decrease. In the later stage, the load power decreases slowly, while the wind power output shows a substantial decline, which lead to a constant increase in the demand of microturbine output power and exchange power.

5.1. Optimization Result Discussion. The intraday optimal dispatch results of RMT and the grid purchase decision from 08:00 to 10:00 are given with an interval of 15 minutes, which is shown in Figure 8. It is observed that the rise in electricity price begins at 8:00, leading to an increase in the cost of exchange power, so the exchange power is decreased and the RMT power is used as the main output power. When the load power rises gradually, the AC/DC distribution network system properly reduces the output power of RMT and increases the exchange power because the RMT cost increases sharply with the rise in power and the RMT output power is limited. The real-time optimal dispatch results of the power of ESS and the QAMT from 08:00 to 09:00 are given with an interval of 5 minutes, which is shown in Figure 9. It is observed that when the load power is low at the starting optimal stage, the storage is mainly charged for the growth of load power in the future. With the constant increase in the load power, the state of storage is transformed to discharge and the power of QAMT also increases rapidly which realizes peak shaving maximally and ensures safe operation of the AC/DC distribution network. The state of charge is shown in Figure 10. It is observed that the state of charge is optimized according to the ESS constraints in the multi-time scale optimal model, the curve of state of charge becomes smoother, and there are no large fluctuations, increasing the ESS usage life and the economy of the AC/DC distribution network.

5.2. Markov Chain Dynamic Scenario Analysis. To verify the effectiveness of the proposed method, the total adjustment value G of the multi-time scale optimal dispatch is analyzed, as shown in (40). The total adjustment value in the intraday optimal dispatch of the Markov chain dynamic scenario model, dynamic scenario model, and Monte Carlo model is shown in Figure 11. It is observed that there is little forecast error observed between the generated scenario and the actual scenario at the beginning due to the high prediction precision. The prediction precision decreases sharply, and the forecast error between the generated scenario and the actual scenario becomes increasingly larger with the growth in the prediction time scale. Scenarios generated by the Monte Carlo method are obtained only by superimposing the perturbation of the normal distribution on the actual load and wind curve, and the total adjustment value increases considerably with the growth in the prediction time scale. Considering the correlation of the original scenario

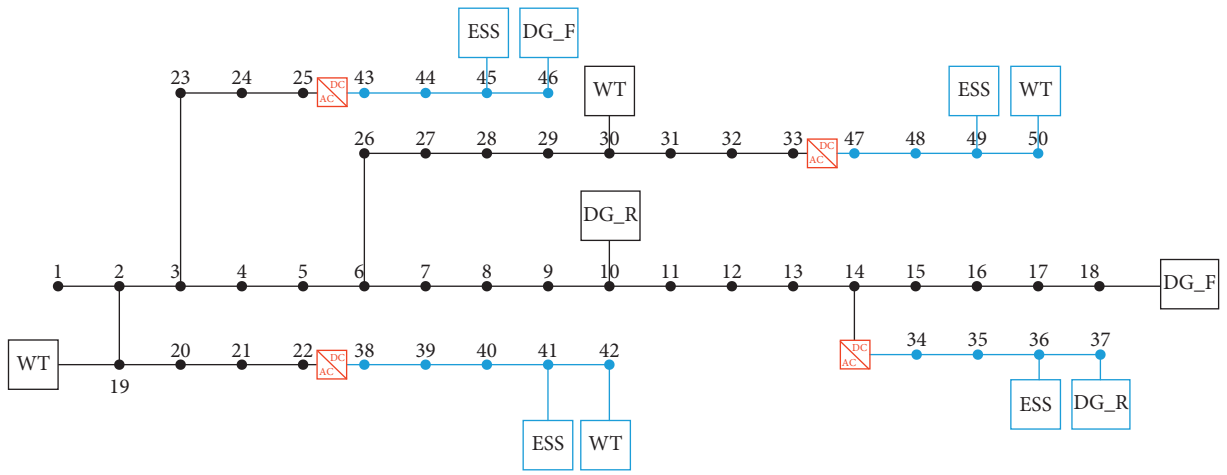

Figure 4: Test system with 50 nodes.

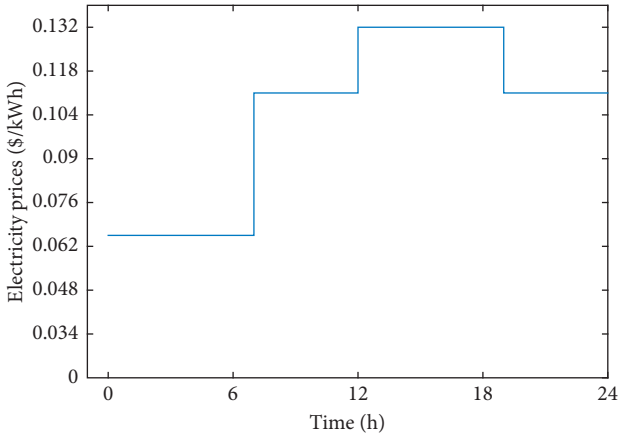

Figure 5: Time-of-use electricity price.

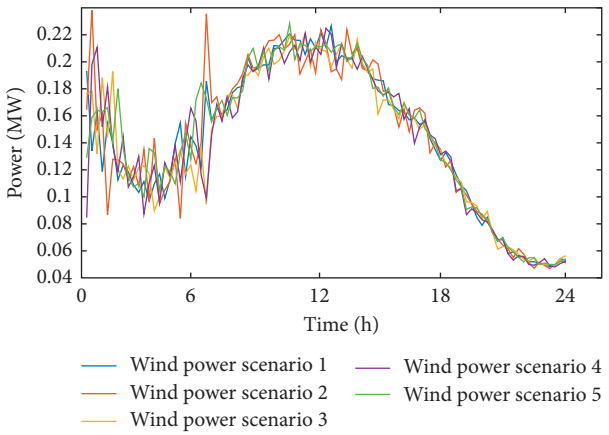

Figure 6: Wind scenario in day-ahead dispatch.

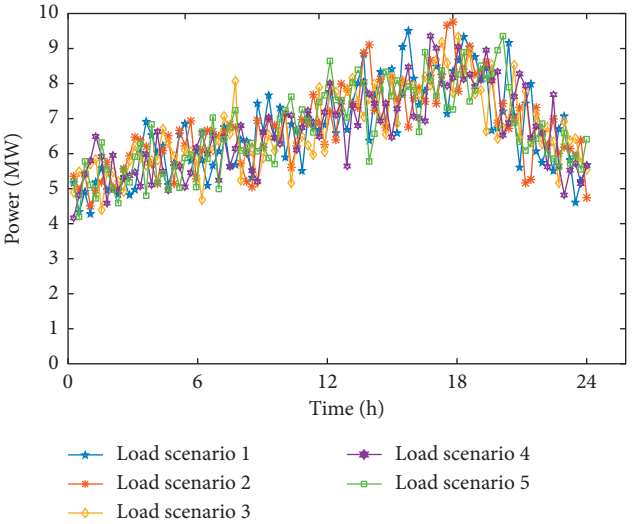

Figure 7: Load scenario in day-ahead dispatch.

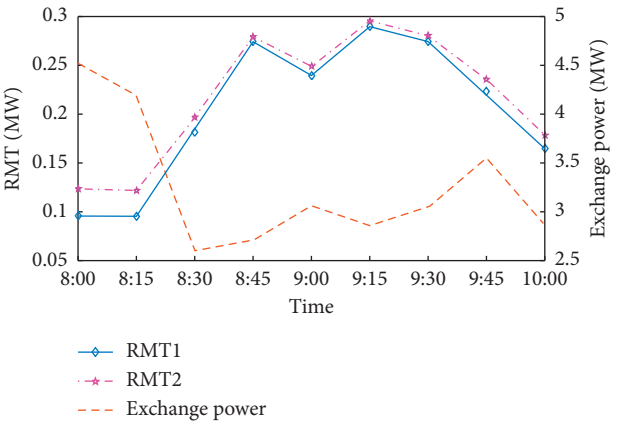

Figure 8: Intraday optimal dispatch result.

with time, the Markov chain is adopted in the Markov chain dynamic scenario method to simulate the change in forecast error with time through the state transfer matrix, so the deviation between the generated scenario and the actual scenario and the adjustment value is relatively small. The total adjustment value of the dynamic scenario method is between the two. The multi-time scale optimal dispatch based on the Markov chain dynamic scenario method can effectively reduce the pressure of the intraday optimal dispatch, verifying the feasibility of the proposed model:

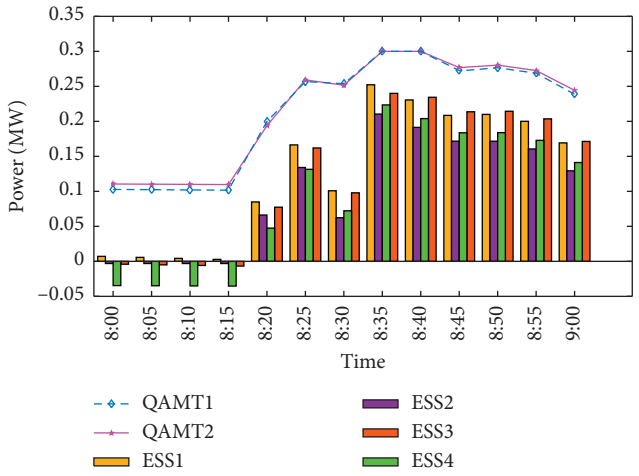

Figure 9: Real-time optimal dispatch result.

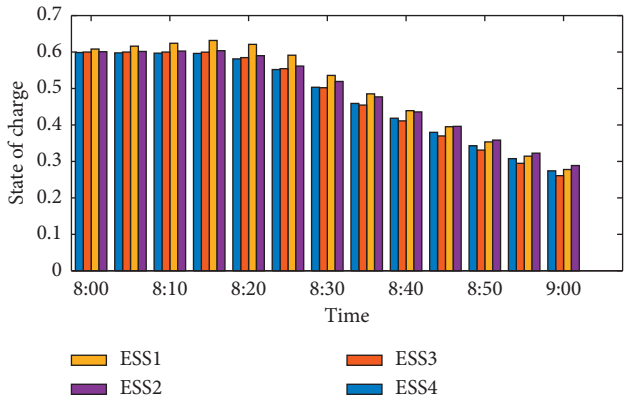

Figure 10: State of charge of ESS.

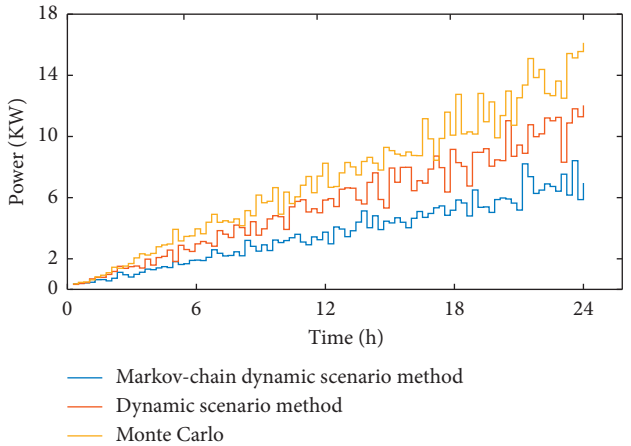

Figure 11: The total adjustment in each optimization model.

$$G = \sum_{t=1}^{T} \sum_{k=1}^{k_c} \frac{\left| P_{\text{dayahead}.t.k} - P_{\text{intraday}.t.k} \right|}{P_{\text{dayahead}.t.k}}, \tag{40}$$

where $P_{\text{dayahead}.t.k}$ is the power of output unit k at moment t in the day-ahead optimal dispatch, $P_{\text{intraday}.t.k}$ is the power of output unit k at moment t in the intraday optimal dispatch, k_c is the number of operation units, and T is the optimal time scale.

To further illustrate the effectiveness of the method proposed in this paper, the coverage ratio of the scenario set over the actual value Π is analyzed, as shown in the following equations:

$$\Pi = \frac{1}{T} \sum_{t=1}^{T} g(P_t), \tag{41}$$

$$g(P_t) = \begin{cases} 1 & P_{t.\min} \le P_t \le P_{t.\max}, \\ 0 & P_t > P_{t.\max}, P_t < P_{t.\min}, \end{cases} \tag{42}$$

where $g(P_t)$ is the probability of covering the actual value for the scenario set at moment t, T is the optimal time scale, P_t is the actual value at moment t, $P_{t.\min}$ is the minimum value of the scenario set, and $P_{t.\max}$ is the maximum value of the scenario set. The range of Π is 0 to 1. The larger the calculation result is, the higher the coverage ratio of the scenario set to the actual value is, the higher the reliability of the solved dispatch schedule is, and the lower the possibility of a failure occurring in the AC/DC distribution network operation is.

Five hundred wind turbine scenarios are generated by the Markov chain dynamic scenario method, the dynamic scenario method, and the Monte Carlo method, respectively. The coverage ratios of these generated scenarios are analyzed, which is shown in Table 1. The coverage ratio of the scenario generated by the Monte Carlo method is lower than those of the other two methods, and the coverage ratio decreases significantly with an increase in the prediction time scale. The scenario generated by the dynamic scenario method has the same high coverage ratio as the Markov chain dynamic scenario method when the prediction time scale is low, but with the continuous growth of the prediction time scale, the coverage ratio of the scenario generated by the dynamic scenario method starts to decrease gradually while the scenarios generated by the Markov chain dynamic scenario method still have high coverage rates.

5.3. MPC Analysis. The result of the intraday optimal dispatch based on MPC and the intraday optimal dispatch without using the MPC method is shown in Figure 12. The intraday optimal dispatch results based on MPC have the same output power trend as the intraday optimal dispatch results without MPC, while the intraday optimal dispatch results without using MPC have large fluctuations. Feedback correction and roll optimization are adopted in the optimal dispatch based on MPC, so the result is relatively smooth, which is more beneficial to the operation of the AC/DC distribution network.

To better compare the results of different optimization methods, the stability of the power of QAMT is analyzed. The output volatility of QAMT is defined as follows:

$$\Gamma = \sum_{i=1}^{N_{DG}} \frac{P_{DG.i}^{\max} - P_{DG.i}^{\min}}{\overline{P}_{DG..i}} \times 100\%, \tag{43}$$

Table 1: Comparative result of the coverage ratio.

Π		Markov chain dynamic scenario method	Dynamic scenario method	Monte Carlo method
Time	1:00–6:00	0.9981	0.9975	0.9471
	7:00–12:00	0.9896	0.9795	0.8995
	13:00–18:00	0.9744	0.9452	0.8451
	19:00–24:00	0.9611	0.8997	0.8071

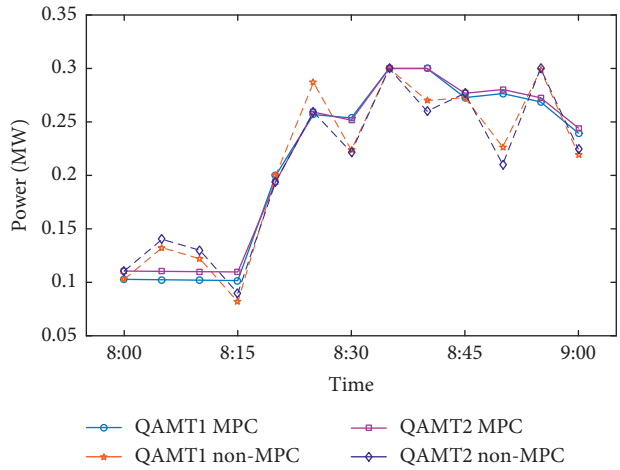

Figure 12: Comparison of real-time dispatch results.

Table 2: Results of different optimization methods.

Optimization method	Volatility (%)	Cost ($)
Non-MPC	66.3	18412.32
MPC1	59.7	18634.25
MPC2	56.1	18787.47

where $P_{DG.i}^{\max}$ and $P_{DG.i}^{\min}$ are the maximum and minimum power of QAMT i in the entire optimal period, respectively, and $\overline{P}_{DG..i}$ is the average power value of QAMT i in the whole optimal period.

The results of these three different optimization methods are compared, as shown in Table 2. MPC1 represents the optimization method that only utilizes roll optimization without feedback correction. MPC2 represents an optimization method utilizing both roll optimization and feedback correction.

Table 2 shows that these three methods have almost the same optimal results. However, as the MPC1 optimization method adopts the roll optimization, the output volatility is 59.7%, which shows a better stability than that of the traditional optimal flow. MPC2 has a lower volatility than MPC1 due feedback correction, which is 56.1%. As a result, MPC2 can ensure that the large power fluctuations in QAMT and ESS will not occur when dealing with the uncertainty and volatility of uncontrollable energy, which is beneficial to maintain the balance of active power in the AC/DC distribution network, improving the stability of system operation.

6. Conclusions

A multi-time scale optimal dispatch model of an AC/DC distribution network based on the Markov chain dynamic scenario method and MPC is proposed. The Markov chain dynamic method is proposed to generate a scenario to address with the fluctuation of uncontrollable energy, and the output power of the unit is solved by adopting roll optimization in intraday optimal dispatch based on MPC, realizing the coordination of day-ahead, intraday, and real-time optimization and the consumption of wind turbine.

(1) As the correlation of the forecast error state with time is considered, the scenario generated by the Markov chain dynamic scenario method has a higher coverage ratio than the scenario generated by the dynamic scenario method when the time scale is long and the solved dispatch schedule using the Markov chain dynamic method has less fluctuations, which improves the stability of the AC/DC distribution network and ensures the safe operation of the system.

(2) All operating units with different adjusting times is used in the power system dispatch by adopting a multi-time scale optimal dispatch model. The operation units with long adjusting times are used in the consumption of uncontrollable distributed energy in the AC/DC distribution network, while the operation units with short start adjusting times are

used to suppress the short-term fluctuation of uncontrollable distributed energy.

(3) As the roll optimization method and feedback correction are used in the process of optimization, MPC has better stability than traditional optimal flow, which can ensure that the output power of QAMT and ESS fluctuates within a certain range, thereby improving the stability and robustness of system operation.

Data Availability

The raw/processed data required to reproduce these findings cannot be shared at this time as the data also form part of an ongoing study.

Conflicts of Interest

The authors declare that they have no conflicts of interest.

References

[1] X. Xu, N. Tai, Y. Hu, W. Wang, F. Zheng, and W. He, "Reliability calculation of AC/DC hybrid distribution network with a solid-state transformer," *The Journal of Engineering*, vol. 2019, no. 16, pp. 3067–3071, 2019.

[2] Y. Wang, N. Zhang, H. Li et al., "Linear three-phase power flow for unbalanced active distribution networks with PV nodes," *CSEE Journal of Power and Energy Systems*, vol. 3, no. 3, pp. 321–324, 2017.

[3] X. Zhu, H. Han, S. Gao, Q. Shi, H. Cui, and G. Zu, "A multi-stage optimization approach for active distribution network scheduling considering coordinated electrical vehicle charging strategy," *IEEE Access*, vol. 6, pp. 50117–50130, 2018.

[4] J. Barr and R. Majumder, "Integration of distributed generation in the volt/VAR management system for active distribution networks," *IEEE Transactions on Smart Grid*, vol. 6, no. 2, pp. 576–586, 2015.

[5] F. Salvadori, C. S. Gehrke, A. C. de Oliveira, M. de Campos, and P. S. Sausen, "Smart grid infrastructure using a hybrid network architecture," *IEEE Transactions on Smart Grid*, vol. 4, no. 3, pp. 1630–1639, 2013.

[6] A. A. Eajal, M. F. Shaaban, K. Ponnambalam, and E. F. El-Saadany, "Stochastic centralized dispatch scheme for AC/DC hybrid smart distribution systems," *IEEE Transactions on Sustainable Energy*, vol. 7, no. 3, pp. 1046–1059, 2016.

[7] M. A. Allam, A. A. Hamad, M. Kazerani, and E. F. El-Saadany, "A novel dynamic power routing scheme to maximize loadability of islanded hybrid AC/DC microgrids under unbalanced AC loading," *IEEE Transactions on Smart Grid*, vol. 9, no. 6, pp. 5798–5809, 2018.

[8] H. W. D. Hettiarachchi, K. T. M. U. Hemapala, and A. G. B. P. Jayasekara, "Review of applications of fuzzy logic in multi-agent-based control system of AC-DC hybrid microgrid," *IEEE Access*, vol. 7, pp. 1284–1299, 2019.

[9] X. Kong, Z. Yan, R. Guo, X. Xu, and C. Fang, "Three-stage distributed state estimation for AC-DC hybrid distribution network under mixed measurement environment," *IEEE Access*, vol. 6, pp. 39027–39036, 2018.

[10] H. Peng, M. Su, S. Li, and C. Li, "Static security risk assessment for islanded hybrid AC/DC microgrid," *IEEE Access*, vol. 7, pp. 37545–37554, 2019.

[11] D. Chen, X. Ji, Y. Yu, X. Bai, and J. Liu, "Unbalanced power flow algorithm for AC&DC hybrid distribution network with diverse-controlled VSC-MTDC converts," *The Journal of Engineering*, vol. 2019, no. 16, pp. 1918–1925, 2019.

[12] J. Wang, A. Botterud, R. Bessa et al., "Wind power forecasting uncertainty and unit commitment," *Applied Energy*, vol. 88, no. 11, pp. 4014–4023, 2011.

[13] Y. Q. Bao, B. B. Wang, Y. Li et al., "Rolling dispatch model considering wind penetration and multi-scale demand response resources," *Proceedings of the CSEE*, vol. 36, no. 17, pp. 4589–4600, 2016.

[14] T. Ding, S. Liu, W. Yuan, Z. Bie, and B. Zeng, "A two-stage robust reactive power optimization considering uncertain wind power integration in active distribution networks," *IEEE Transactions on Sustainable Energy*, vol. 7, no. 1, pp. 301–311, 2016.

[15] X.-Y. Ma, Y.-Z. Sun, and H.-L. Fang, "Scenario generation of wind power based on statistical uncertainty and variability," *IEEE Transactions on Sustainable Energy*, vol. 4, no. 4, pp. 894–904, 2013.

[16] X. Lei, T. Huang, Y. Yang, Y. Fang, and P. Wang, "A bi-layer multi-time coordination method for optimal generation and reserve schedule and dispatch of a grid-connected microgrid," *IEEE Access*, vol. 7, pp. 44010–44020, 2019.

[17] L. Guanqun, F. Yongshen, Q. Dagong, S. Guangmin, and S. Xiaoqing, "Research on multi-objective optimal joint dispatching of wind-thermal-hydro power in multi time scales," in *Proceedings of the 2016 IEEE PES Asia-Pacific Power and Energy Engineering Conference (APPEEC)*, pp. 1832–1839, Xi'an, China, October 2016.

[18] C. L. Floch, S. Bansal, C. J. Tomlin, S. J. Moura, and M. N. Zeilinger, "Plug-and-play model predictive control for load shaping and voltage control in smart grids," *IEEE Transactions on Smart Grid*, vol. 10, no. 3, pp. 2334–2344, 2019.

[19] G. Valverde and T. Van Cutsem, "Model predictive control of voltages in active distribution networks," *IEEE Transactions on Smart Grid*, vol. 4, no. 4, pp. 2152–2161, 2013.

[20] H. Zhao, Q. Wu, Q. Guo, H. Sun, and Y. Xue, "Distributed model predictive control of a wind farm for optimal active power control—part II: implementation with clustering-based piece-wise affine wind turbine model," *IEEE Transactions on Sustainable Energy*, vol. 6, no. 3, pp. 840–849, 2015.

[21] L. Dong, H. Chen, T. J. Pu et al., "Multi-time scale dynamic optimal dispatch in active distribution network based on model predictive control," *Proceedings of the CSEE*, vol. 36, no. 17, pp. 4609–4617, 2016.

[22] S. Tewari, C. J. Geyer, and N. Mohan, "A statistical model for wind power forecast error and its application to the estimation of penalties in liberalized markets," *IEEE Transactions on Power Systems*, vol. 26, no. 4, pp. 2031–2039, 2011.

[23] A. Shamshad, M. Bawadi, W. Wanhussin, T. Majid, and S. Sanusi, "First and second order Markov chain models for synthetic generation of wind speed time series," *Energy*, vol. 30, no. 5, pp. 693–708, 2005.

[24] M. I. Garcia-Planas and T. Gongadze, "Wind profile prediction using linear Markov chains: a linear algebra approach," *IEEE Latin America Transactions*, vol. 16, no. 2, pp. 536–541, 2018.

[25] B. M. Zhang, W. C. Wu, T. Y. Zheng et al., "Design of a multi-time scale coordinated active power dispatching system for accommodating large scale wind power penetration," *Automation of Electric Power Systems*, vol. 35, no. 1, pp. 1–6, 2011.

[26] X. Ma, R. P. Guo, L. Wang et al., "Day-ahead optimal dispatch model of AC/DC active distribution network based on second-order cone programming," *Automation of Electric Power System*, vol. 42, no. 22, pp. 144–150, 2018.

[27] E. F. Camacho and C. Bordons, *Model Predictive Control*, vol. 204, pp. 14–31, Springer-Verlag, New York, NY, USA, 2004.

[28] S. X. Wang, S. J. Chen, and S. G. Xie, "Security-constrained coordinated economic dispatch of energy storage systems and converter stations for AC/DC distribution networks," *Automation of Electric Power Systems*, vol. 41, no. 11, pp. 85–91, 2017.

[29] L. Wu, M. Shahidehpour, and Z. Li, "Comparison of scenario-based and interval optimization approaches to stochastic SCUC," *IEEE Transactions on Power Systems*, vol. 27, no. 2, pp. 913–921, 2012.